Multidimensional estimation of cardiac arrhythmia potential across space and time

Francisco Sahli Costabal[1], Kinya Seo[2], Euan Ashley[2,3], Ellen Kuhl[1,4]

[1] *Department of Mechanical Engineering, Stanford University, Stanford, CA 94305, USA*
[2] *Department of Medicine, Stanford University, Stanford, CA 94305, USA*
[3] *Department of Pathology, Stanford University, Stanford, CA 94305, USA*
[4] *Department of Bioengineering, Stanford University, Stanford, CA 94305, USA*

All medications have adverse effects. Among the most serious of these are cardiac arrhythmias[1]. The current safety evaluation for cardiac toxicity involves interrogating effects of the drug on the delayed rectifier potassium current in single cells[2] and the QT interval in healthy volunteers[3]. However, this paradigm for drug safety evaluation is costly[4], lengthy[5], conservative[3], and impede efficient drug development[6]. Here we combine multiscale experiment and simulation, high-performance computing, and machine learning to create a multidimensional risk estimator to quickly and reliably stratify new and existing drugs according to their pro-arrhythmic potential. We capitalize on recent developments in machine learning and integrate information across ten orders of magnitude in space and time to provide a holistic picture of the effects of drugs, either individually or in combination with other drugs. We show, both experimentally and computationally, that drug-induced arrhythmias are dominated by the interplay between two currents with opposing effects: the rapid delayed rectifier potassium current and the L-type calcium current. Using Gaus-

sian process classification, we create a classifier that stratifies drugs into safe and arrhythmic domains for any combinations of these two currents. We demonstrate that our classifier correctly identifies the risk categories of 23 common drugs, exclusively on the basis of their concentrations at 50% current block. Our new risk estimator explains under which conditions blocking the L-type calcium current can delay or even entirely suppress arrhythmogenic events. Using machine learning in drug safety evaluation can provide a more accurate and comprehensive mechanistic assessment of the pro-arrhythmic potential of new drugs. Our study paves the way towards establishing science-based criteria to accelerate drug development, design safer drugs, and reduce heart rhythm disorders.

Many drugs, not just cardiac drugs, interact with specific ion channels in the heart and can induce serious rhythm disorders[1]. Indeed, the major focus of FDA toxicity testing is the pro-arrhythmic potential of a drug, as determined by its effect on cardiac repolarization. Specifically, the approval of a new drug requires assessing its impact on the rapid component of the delayed rectifier potassium current in single cell experiments[2] and on the duration of ventricular activity in animal models and in healthy human volunteers[3]. Unfortunately, the high cost[4] and long time to test new compounds[5] acts as an impediment to the discovery of new drugs[7]. Further, the limited window provided by these criteria onto pro-arrhythmic potential generates false-positives while at the same time preventing many potentially useful drugs from ever reaching the market[6]. Computational modeling[8] and machine learning could significantly accelerate the early stages of drug development, guide the design of safe drugs, and help reduce drug-induced rhythm disorders[9].

All pharmacological agents have the potential to impact cardiac repolarization and, with it, cause torsades de pointes, a ventricular arrhythmia characterized by rapid, irregular patterns in the electrocardiogram[10]. Most episodes of torsades de pointes begin spontaneously and revert to normal sinus rhythm within a few seconds; but some persist, degenerate into ventricular fibrillation, and lead to sudden cardiac death, even in patients with structurally normal hearts[11]. Predicting this potentially fatal heart rhythm is challenging given the complex interplay between genetic predisposition and medications.

While using machine learning in the early stages of drug design, target selection, and high throughput screening is almost standard today, the potential of machine learning in the later stages of drug development, toxicity screening, and risk stratification has not been recognized to its full extent[12]. There is a general agreement between clinical researchers, pharmaceutical companies, and regulatory agencies that computational tools should play a more central role in the pro-arrhythmic risk assessment of new drugs[13–15]. However, current efforts focus exclusively on classifiers at the single cell level and ignore ventricular heterogeneity and the interaction of different cell types across the entire heart[16]. We have recently proposed a novel exposure-response simulator that allows us visualize how different drugs modulate the cardiac electrophysiology across ten orders of magnitude in space and time[17]. Here, we combine this simulator with machine learning techniques[18] to seamlessly integrate experimental and computational data from the protein, cellular, tissue, and organ scales to assess cardiac toxicity during pharmacological profiling[19] (Figure 1).

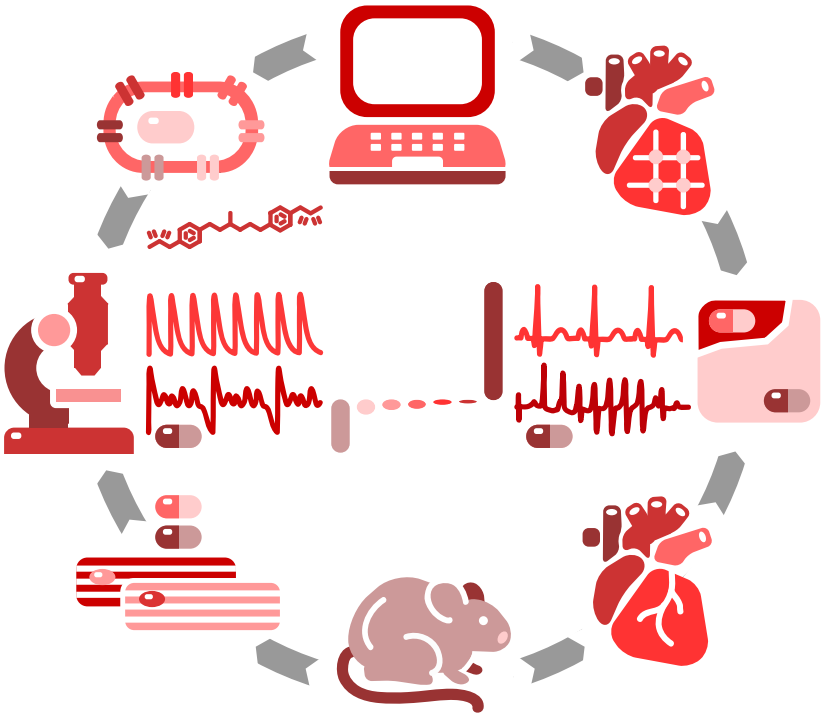

Figure 1: **Hybrid computational-experimental approach to characterize the pro-arrhythmic potential of existing and new drugs.** We characterize calcium transients in cardiomyocytes in response to drugs, both computationally (top) and experimentally (bottom) and identify the ion channels that most likely generate early afterdepolarizations (left). We screen the blockade space of the two most relevant channels and identify the pro-arrhythmic classification boundary using high performance computing and machine learning (center). We validate our approach using electrocardiograms in simulations and isolated perfused hearts (right). We demonstrate the potential of our classifier by risk stratifying 23 drugs and comparing the result against their reported risk categories.

Increasing evidence suggests that early afterdepolarizations are a precursor of torsades de pointes at the cellular level[20,21]. To identify which ion channels have the most significant impact on the appearance of early afterdepolarizations, we model single midwall cells and block seven ion channels and monitoring for early afterdepolarizations. Figure 2, top left, illustrates these seven ion channels within the O'Hara Rudy model for ventricular cardiomyocytes[22]. We fit a logistic regression and extract the marginal effects to quantify the effect of each channel blockade on the probability of early afterdepolarizations. Our results show that of the seven channels, the rapid delayed rectifier potassium current I_{Kr} and the L-type calcium current I_{CaL} have the most pronounced effects on early afterdepolarizations. Yet, these two currents display opposite effects: The current I_{Kr} significantly increases the risk of early afterdepolarizations, while I_{CaL} decreases the risk. To validate these findings, we isolate rat ventricular cardiomyocytes and expose them to the drug dofetilide, which selectively blocks I_{Kr}. We record calcium fluorescence and compare it to the calcium transients predicted by the computational model of human ventricular endocardial cells. Figure 2, middle row, shows the development of early afterdepolarizations in the presence of the drug dofetilide, both in isolated rat cardiomyocytes and in the single cell model. In both cases, the relationship between the probability of early afterdepolarizations and the concentration of the drug is dose-dependent: Increasing the dose of dofetilide increases the probability of early afterdepolarizations. We select the two ion channels that most strongly enhance and prevent early afterdepolarizations, I_{Kr} and I_{CaL} to study torsades de pointes. We use our high resolution human heart model[23] to simulate the effect of combined I_{Kr} and I_{CaL} block at different concentrations[17]. We

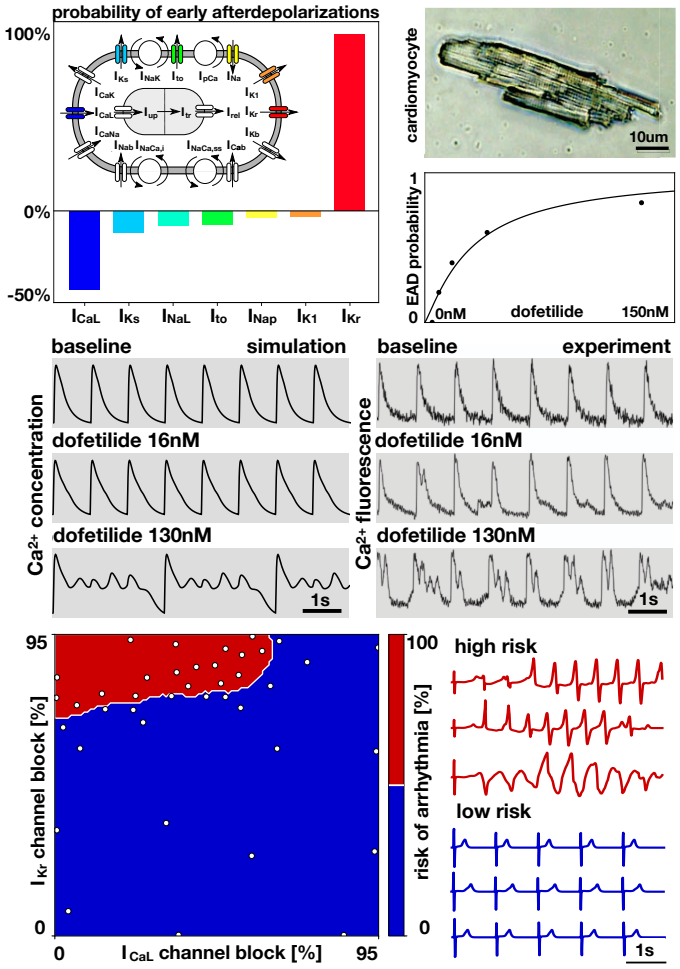

Figure 2: **Effects of ion channel blockade on cell and heart arrhythmic behavior.** Top left, sensitivity analysis of early afterdepolarizations. Positive/negative values imply that blocking this ion channel enhances/prevents early afterdepolarizations. Top right, isolated cardiomyocyte and probability to develop early afterdepolarizations in response to the drug dofetilide. Middle row, calcium transients in response to dofetilide in computational simulation, left, and experiment, right. Bottom row, screening the parameter space of I_{Kr} and I_{CaL} block reveals the pro-arrhythmic boundary. Blue electrocardiograms display normal sinus rhythm; red electrocardiograms spontaneously develop torsades de pointes.

adopt a particle learning Gaussian process classifier with adaptive sampling to efficiently explore the parameter space, probing the points of maximum entropy[24]. Figure 2, bottom right, summarizes the results of our pro-arrhythmic risk classification. The vertical axis reveals the pro-arrhythmic risk for a selective block of the I_{Kr}: At a critical I_{Kr} block of 70%, the risk classification changes from low, shown in blue, to high, shown in red, and the heart will spontaneously develop torsades de pointes. Moving horizontally to the right modulates the pro-arrhythmic risk for a combined block with I_{CaL}: When combining I_{Kr} and I_{CaL} block, the critical I_{Kr} block increases above 70%. Beyond an I_{CaL} block of 60%, the heart will not develop arrhythmia, no matter how high the I_{Kr} block.

To validate these predictions we took advantage of an isolated Langendorff perfused rat heart preparation exposed to two different drugs, dofetilide, which selectively blocks the I_{Kr} and nifedipine, which selectively blocks I_{CaL}. Figure 3 shows that for the baseline case without drugs, both the computational model and experimental system display normal sinus rhythm, first row. Blocking I_{Kr} by administering dofetilide beyond a critical concentration induces arrhythmias both computationally and experimentally, second row, an observation that agrees well with the single cell simulation and experiment in Figure 2, middle row. Additionally blocking I_{CaL} by co-administering a small concentration of nifedipine markedly alters the excitation pattern both computationally and experimentally, but still triggers irregular beats. Increasing the I_{CaL} block by co-administering a large concentration of nifedipine removes the risk of arrhythmias both computationally and experimentally, the hearts excite at a regular pattern.

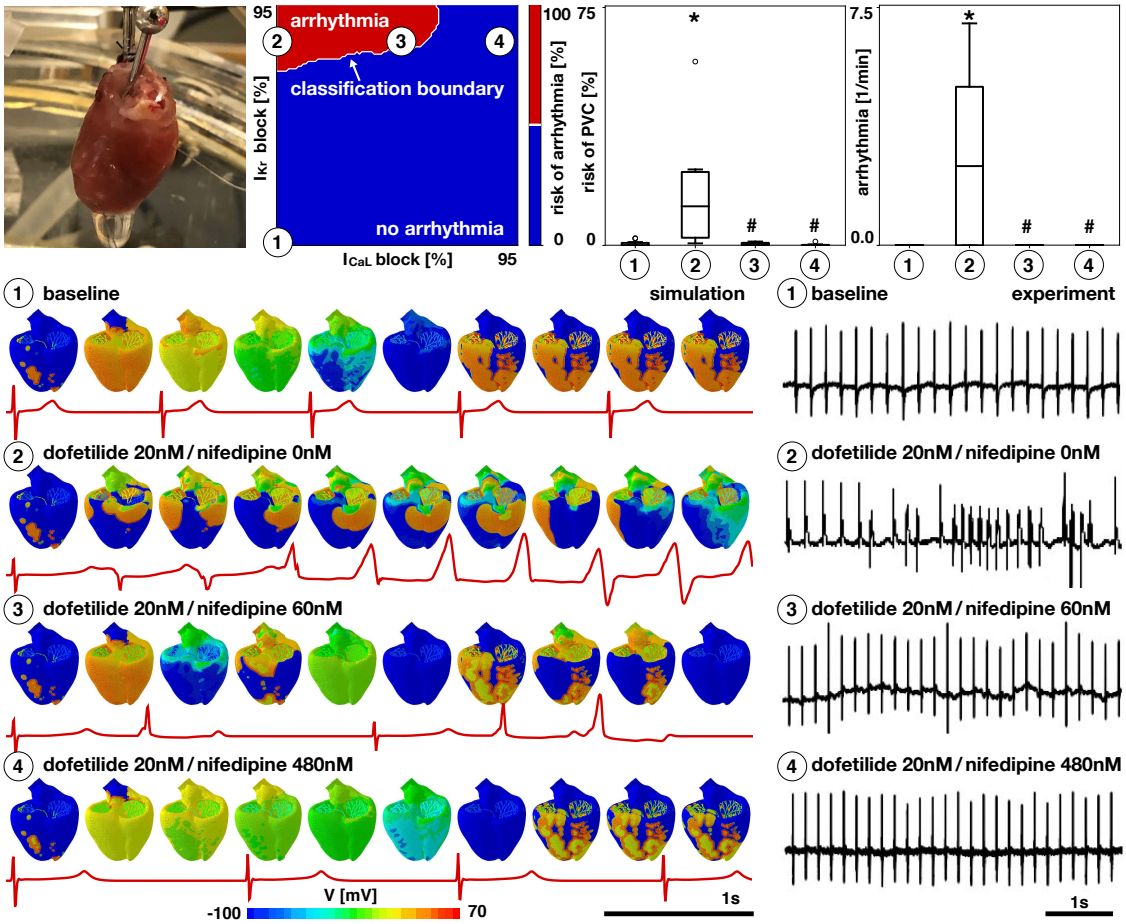

Figure 3: **Ventricular arrhythmias in whole heart simulation and Langendorff perfused hearts.** Preparation of isolated rat heart, top left, four drug concentrations visualized in the risk classifier, top middle, and risk of premature ventricular contractions and arrhythmias in response to varying concentrations of drugs dofetilide and nifedipine (n$\geq$6, $*$ p$<$0.05 compared to ①, # p$<$0.05 compared to ②), top right. Dofetilide selectively blocks I_{Kr}; nifedipine selectively blocks I_{CaL}. Electrocardiograms in response to dofetilide combined with nifedipine in the computational simulation, bottom left, and experiment, bottom right.

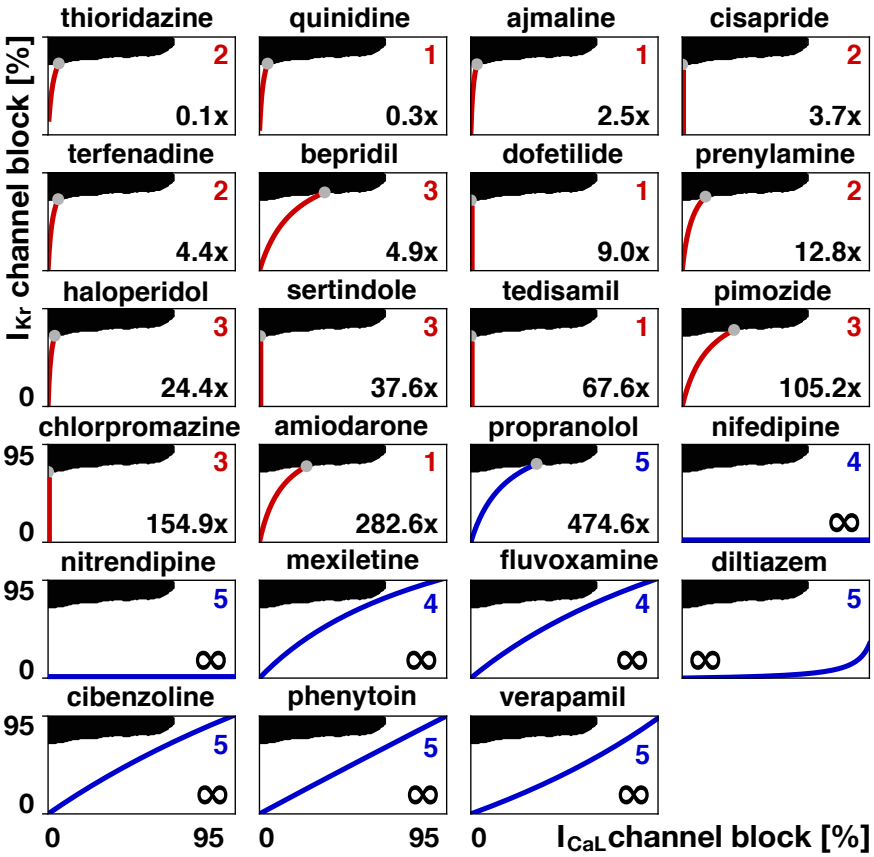

Figure 4: **Risk stratification of 23 drugs using our pro-arrythmic risk classifier.** Black and white regions indicate arrhythmic and non-arrhythmic regimes; red and blue curves indicate high and low risk drugs; gray dots and numbers indicate the critical concentration at which the curves cross the classification boundary as predicted by our pro-arrythmic risk classification in Figure 2. Numbers from 1 to 5 indicate the reported torsadogenic risk[2,13]; red and blue colors of the numbers indicate torsadogenic and non-torsadogenic compounds[15].

To validate our approach, we calculate the critical concentrations for 23 drugs using the risk assessment classifier in Figure 2, bottom left. The individual block-concentration characteristics for each drug[1,13,25] map onto a trajectory in the $I_{\mathrm{Kr}}/I_{\mathrm{CaL}}$ plane of the risk estimator. The intersection of this trajectory with the classification boundary defines the critical drug concentration. Curves that never cross the classification boundary indicate a safe drug. Figure 4 demonstrates that our classification boundary can reliably stratify the risk of 23 common drugs. Fourteen drugs are classified as high risk drugs. Nine drugs are classified as low risk drugs. Of those, propranolol crosses the classification boundary at 474x. All other drugs low risk drugs never cross the classification boundary.

Current drug screening paradigms are expensive, time consuming, and conservative. Here we propose a new approach that integrates knowledge from the ion channel, single cell, and whole heart levels via computational modeling and machine learning to reliably predict the cardiac toxicity of new and existing drugs. Our results are based on a rigorous sensitivity analysis that identifies a pair of counteracting ion channels, I_{Kr} and I_{CaL}, that play the most significant role in enhancing and reducing arrhythmogenic risk. We combine multiscale experiments, multiscale simulation, high-performance computing, and machine learning to create a multi-dimensional risk estimator that allows us to quickly and reliably identify the pro-arrhythmic potential of existing and new drugs, either in isolation or combined with other drugs. Collectively, these new insights are significant in the development of new compounds. Our efforts significantly extend current initiatives by pharmaceutical industries, clinical researchers, and regulatory agencies with the common goal to develop

a new testing paradigm for a more accurate and comprehensive mechanistic assessment of new drugs.

1. Crumb, W. J., Vicente, J., Johannesen, L. & Strauss, D. G. An evaluation of 30 clinical drugs against the comprehensive in vitro proarrhythmia assay (cipa) proposed ion channel panel. *Journal of pharmacological and toxicological methods* **81**, 251–262 (2016).

2. Redfern, W. S. *et al.* Relationships between preclinical cardiac electrophysiology, clinical QT interval prolongation and torsade de pointes for a broad range of drugs: Evidence for a provisional safety margin in drug development. *Cardiovascular Research* **58**, 32–45 (2003).

3. Gintant, G., Sager, P. & Stockbridge, N. Evolution of strategies to improve preclinical cardiac safety testing. *Nature Reviews. Drug Discovery* 1–15.

4. Maxmen, A. Big pharma's - cost-cutting challenger. *Nature* **536**, 388–390 (2016).

5. DiMasi, J. A., Hansen, R. W. & Grabowski, H. G. The price of innovation: new estimates of drug development costs. *Journal of health economics* **22**, 151–185 (2003).

6. Stockbridge, N., Morganroth, J., Shah, R. R. & Garnett, C. Dealing with global safety issues. *Drug Safety* **36**, 167–182 (2013).

7. Colatsky, T. *et al.* The comprehensive in vitro proarrhythmia assay (CiPA) initiative – Update on progress. *Journal of Pharmacological and Toxicological Methods* **81**, 15–20 (2016).

8. Trayanova, N. From genetics to smart watches: developments in precision cardiology. *Nature Reviews Cardiology* **16**, 72–73 (2019).

9. Niederer, S. A., Lumens, J. & Trayanova, N. A. Computational models in cardiology. *Nature Reviews Cardiology* 1 (2018).

10. Dessertenne, F. La tachycardie ventriculaire a deux foyers opposes variables. *Archives des Maladies du Coeur et des Vaisseaux* **2**, 263–272 (1966).

11. Gupta, A., Lawrence, A. T., Krishnan, K., Kavinsky, C. J. & Trohman, R. G. Current concepts in the mechanisms and management of drug-induced qt prolongation and torsade de pointes. *American heart journal* **153**, 891–899 (2007).

12. Yang, H., Sun, L., Li, W., Liu, G. & Tang, Y. In silico prediction of chemical toxicity for drug design using machine learning methods and structural alerts. *Frontiers in chemistry* **6**, 30 (2018).

13. Mirams, G. *et al.* Simulation of multiple ion channel block provides improved early prediction of compounds' clinical torsadogenic risk. *Cardiovascular Research* **91**, 53–61 (2011).

14. Parikh, J., Gurev, V. & Rice, J. J. Novel two-step classifier for torsades de pointes risk stratification from direct features. *Frontiers in pharmacology* **8**, 816 (2017).

15. Lancaster, M. & Sobie, E. Improved prediction of drug-induced torsades de pointes through simulations of dynamics and machine learning algorithms. *Clinical pharmacology and therapeutics* **100** (2016).

16. Sahli Costabal, F., Yao, J., Sher, A. & Kuhl, E. Predicting critical drug concentrations and torsadogenic risk using a multiscale exposure-response simulator (2018).

17. Sahli Costabal, F., Yao, J. & Kuhl, E. Predicting the cardiac toxicity of drugs using a novel multiscale exposureresponse simulator. *Computer Methods in Biomechanics and Biomedical Engineering* (2018).

18. Perakakis, N., Yazdani, A., Karniadakis, G. E. & Mantzoros, C. Omics, big data and machine learning as tools to propel understanding of biological mechanisms and to discover novel diagnostics and therapeutics. *Metabolism: clinical and experimental* **87**, a1–a9 (2018). Exported from https://app.dimensions.ai on 2019/03/15.

19. Costabal, F. S., Matsuno, K., Yao, J., Perdikaris, P. & Kuhl, E. Machine learning in drug development: Characterizing the effect of 30 drugs on the qt interval using gaussian process regression, sensitivity analysis, and uncertainty quantification. *Computer Methods in Applied Mechanics and Engineering* **348**, 313 – 333 (2019).

20. Qu, Z. *et al.* Early afterdepolarizations in cardiac myocytes: beyond reduced repolarization reserve. *Cardiovascular research* **99**, 6–15 (2013).

21. Song, Z., Qu, Z. & Karma, A. Stochastic initiation and termination of calcium-mediated triggered activity in cardiac myocytes. *Proceedings of the National Academy of Sciences* **114**, E270–E279 (2017).

22. O'Hara, T., Virág, L., Varró, A. & Rudy, Y. Simulation of the undiseased human cardiac ventricular action potential: model formulation and experimental validation. *PLoS Computational Biology* **7**, e1002061 (2011).

23. Baillargeon, B., Rebelo, N., Fox, D., Taylor, R. & Kuhl, E. The Living Heart Project: A robust and integrative simulator for human heart function. *European Journal of Mechanics. A: Solids* **48**, 38–47 (2014).

24. Gramacy, R. B. & Polson, N. G. Particle Learning of Gaussian Process Models for Sequential Design and Optimization. *Journal of Computational and Graphical Statistics* **20**, 102–118 (2017).

25. Johnstone, R. H., Bardenet, R., Gavaghan, D. J. & Mirams, G. R. Hierarchical bayesian inference for ion channel screening dose-response data. *Wellcome open research* **1** (2016).

Acknowledgments

This study was supported by the Stanford School of Engineering Fellowship (F.S.C.), the Becas Chile-Fulbright Fellowship (F.S.C.), the Extreme Science and Engineering Discovery Environment XSEDE (E.K.), the Stanford Bio-X IIP Seed Grant program (E.A. and E.K.), and the National Institutes of Health Grant U01-HL119578 (E.K.).

Author contributions

F.S.C. performed the simulations; K.S. performed the experiments, F.S.C., K.S., E.A., and E.K. designed the research, analyzed the data, and wrote the manuscript.

Methods

All studies were approved by the Stanford Administrative Panel on Laboratory Animal Care and conform to the Guide for the Care and Use of Laboratory Animals published by the National Institutes of Health.

* Simulating action potentials in ventricular cardiomyocytes We modeled the temporal evolution of the transmembrane potential ϕ using an ordinary differential equation,

$$\dot{\phi} = -I_{\mathrm{ion}}/C_{\mathrm{m}}\,, \tag{1}$$

where C_{m} is the membrane capacitance and $I_{\mathrm{ion}}(\phi, \boldsymbol{q})$ is the ionic current, which we represented as a function of the transmembrane potential ϕ and a set of state variables $\boldsymbol{q}$[1]. The state variables obey ordinary differential equations, $\dot{\boldsymbol{q}} = \boldsymbol{g}(\phi, \boldsymbol{q})$, as functions of the transmembrane potential ϕ and their current values $\boldsymbol{q}$[2]. For our single cell simulations, we used ventricular cardiomyocytes with 15 ionic currents and 39 state variables[3],

$$\begin{aligned} I_{\mathrm{ion}} = I_{\mathrm{Kr}} &+ I_{\mathrm{Ks}} + I_{\mathrm{K1}} + I_{\mathrm{CaL}} + I_{\mathrm{Na}} \\ &+ I_{\mathrm{CaNa}} + I_{\mathrm{CaK}} + I_{\mathrm{Cab}} + I_{\mathrm{Nab}} + I_{\mathrm{Kb}} \\ &+ I_{\mathrm{to}} + I_{\mathrm{NaK}} + I_{\mathrm{pCa}} + I_{\mathrm{NaCa,i}} + I_{\mathrm{NaCa,ss}}\,, \end{aligned} \tag{2}$$

with a minor modification[4] of the fast sodium current I_{NaP}[5]. We parameterized the model for human midwall cells[3], and modeled the effect of drugs by selectively blocking the relevant ionic currents I_{ion}[6]. For a desired concentration C, for each current i, we calculate the fractional block β_{i} using a Hill-type model parameterized with data from patch clamp

electrophysiology[7,8], and scale the ionic current I_{i} by this fractional block[9],

$$I_{\mathrm{i}}^{\mathrm{drug}} = [\,1 - \beta_{\mathrm{i}}\,]\, I_{\mathrm{i}} \quad \text{with} \quad \beta_{\mathrm{i}} = [\,1 + [\,C/IC_{50}\,]\,]^{-1}\,. \tag{3}$$

We studied the relative importance of seven ion channels, $I_{\mathrm{CaL}}, I_{\mathrm{K1}}, I_{\mathrm{Kr}}, I_{\mathrm{Ks}}, I_{\mathrm{NaL}}, I_{\mathrm{NaP}}$, and I_{to} on inducing early afterdepolarizations. To achieve a steady state, we paced the cells for 600 cycles at a frequency of 1Hz. We defined the presence of early afterdepolarizations as the occurrence of a change in potential greater than 0.1mV/ms between the 50 and 1000ms of the last two recorded cycles[10]. We used a latin hypercube design to perform 500 simulations and systematically varied the block of the seven ion channels between 0 and 95%. Then, we labeled the results depending on the presence or absence of early afterdepolarizations. We fit a logistic regression and computed the marginal effects, which correspond to the derivative of the output of the regression with respect to the ion channel block. We normalized the results by the maximum value.

* Simulating electrocardiograms in human hearts To pass information across the scales, we created an ultra high resolution finite element model of the human heart[9] that represents individual ion channel dynamics through local ordinary differential equations at the integration point level and action potential propagation through global partial differential equations at the node point level[11]. The basis of this model is the classical monodomain model that characterizes the spatio-temporal evolution of the transmembrane potential ϕ through the following partial differential equation,

$$\dot{\phi} = \mathrm{div}(\boldsymbol{D} \cdot \nabla\phi) - I_{\mathrm{ion}}/C_{\mathrm{m}}\,. \tag{4}$$

In addition to the local source term $I_{\mathrm{ion}}/C_{\mathrm{m}}$ from equation (1), the transmembrane potential depends on the global flux term div$(\boldsymbol{D} \cdot \nabla\phi)$, where $\boldsymbol{D}$ is the conductivity tensor that accounts for a fast signal propagation of $D^{\parallel}$ parallel to the fiber direction $\boldsymbol{f}$ and a slow signal propagation of $D^{\perp}$ perpendicular to it[1],

$$\boldsymbol{D} = D^{\parallel}\, \boldsymbol{f} \otimes \boldsymbol{f} + D^{\perp}\, [\, \boldsymbol{I} - \boldsymbol{f} \otimes \boldsymbol{f}\,]\,. \tag{5}$$

We used the O'Hara Rudy model[3] from equation (2) for all ventricular cells and the Stewart model[12] for all Purkinje cells. We discretized the monodomain equation (4) in time using finite differences and in space using finite elements[1] and introduced the transmembrane potential as a degree of freedom at the node point level and all state variables as local degrees of freedom at the integration point level[2]. We solved the resulting system of equations using the finite element software package Abaqus[13] with an explicit time integration scheme. We discretized our simulation window of five healthy heart beats in time using 1.0M equidistant time steps of $\Delta t = 0.005$ms. We discretized our human heart model[14] in space using 6.9M regular trilinear hexagonal elements with a constant edge length of $h = 0.3$mm. This results in 7.5M global degrees of freedom and 0.3G local internal variables[11].

* Using machine learning tools to sample the parameter space To quickly and efficiently sample the parameter space for a wide range of conditions and a wide variety of drugs we combine our computational models with machine learning techniques[15,16]. Briefly, to characterize ventricular fibrillation, we performed $n = 40$ human heart simulations and employed a particle learning method to systematically sample the classification boundary

within the parameter space. To identify the boundary that divides the arrhythmic and non-arrhythmic domains, we used a Gaussian process classifier and adaptively sampled the point of maximum entropy[17]. We generated the first $n = 10$ samples from a latin hypercube design, and sampled the remaining $n = 30$ samples adaptively. Our results suggest that $n = 40$ simulations are sufficient to reliably identify the classification boundary.

* Classifying drugs into risk categories We classified 23 drugs into high and low risk, based on our pro-arrhythmic risk estimator in Figure 2, bottom right, and validated our approach against the known risk classification of these drugs. To select the compounds, we began with a list 31 drugs[7] for which the concentration block is thoroughly characterized. From these 31 drugs, we only considered those for which 70% or more of the published studies agreed on their risk classification[18,19], and did not consider the remaining eight controversial drugs. Table 1 summarizes the IC_{50} values used to compute the degree of blockade of the L-type calcium current I_{CaL} and the rapid delayed rectifier potassium current I_{Kr}[7].

* Measuring calcium transients in isolated cardiomyocytes To characterize calcium transients, we isolated ventricular cardiomyocytes from the hearts of male Sprague Dawley rats with a weight of 250-300g (Charles River, Massachusetts). We anesthetized the rats with inhaled isoflurane and quickly removed the hearts from the chest after euthanasia. We retrograde-perfused the hearts with Ca^{2+}-free Tyrode buffer (140mM NaCl, 5.4mM KCl, 0.33mM NaH_2PO_4, 0.5mM $MgCl_2$, 11mM glucose, and 5mM HEPES at pH7.4) at 1.0ml/min for three minutes, followed by an enzyme solution containing collagenase

(1.0mg/ml collagenase type II, Worthington), protease (0.05mg/ml, type XIV, Sigma), and 0.1mM Ca^{2+} for seven minutes. To harvest the cardiomyocytes, we cut the ventricular tissue into small pieces and filtered it with a 250μm nylon mesh. We gradually increased the calcium concentration of the Tyrode solution to 1.0mM for the physiologic analysis and incubated the cardiomyocytes for 15 minutes with 1μM Fura-2-AM (Invitrogen, California) in Tyrode (1.0mM, Ca^{2+}). We mounted the cardiomyocytes into a recording chamber on the stage of an Olympus IX-71 inverted microscope (Olympus, New York) where we stimulated them electrically at a frequency of 0.5Hz. Using a galvanometer-driven mirror (HyperSwitch, IonOptix, Massachusetts), we excited Fura-2 at a wavelength of 340/380nm and recorded the emission at 510nm using a photomultiplier (IonOptix, Massachusetts). After five minutes of incubation with the drug dofetilide at concentrations of 4nM, 8nM, 16nM, 38nM, 130nM, we recorded cardiomyocyte calcium fluorescence at 250Hz for eight minutes for n=6 cells each and analyzed the recordings in real time.

* Recording electrocardiograms in perfused Langendorff hearts To record electrocardiograms, we harvested the hearts of male Sprague Dawley rats with a weight of 250-300g (Charles River, Massachusetts). We excised the hearts from anesthetized rats (2.5% isoflurane in 95% oxygen and 5% carbon dioxide), immediately cannulated the aorta, connected it to a constant pressure perfusion Langendorff system (Harvard Apparatus, Massachusetts) with Krebs solution (118mM NaCl, 4.75mM KCl, 25mM $NaHCO_3$, 1.2mM KH_2PO_4, 1.2mM $MgSO_4$, 1.5mM $CaCl_2$, 11mM glucose, and 2mM Pyruvate), warmed to 37° C, and bubbled with 95% oxygen and 5% carbon dioxide. We instrumented the spon-

taneously beating hearts with ECG electrodes located at the apex and base. After ten minutes of equilibration, we switched the perfusion system to a reservoir to expose the hearts to selected concentrations of dofetilide and nifedipine for a period of five minutes. For $n \geq 6$ hearts in each group, we recorded the ECG by Animal Bio Amp (AD Instruments, Colorado) and monitored it continuously throughout the experiment and the a washout period using a Power Lab system (AD Instruments, Colorado).

* Experimentally characterizing the effect of drugs We characterized the occurrence of arrhythmias in both the isolated cardiomyocytes and the perfused hearts. For the isolated cardiomyocytes, we counted an arrhythmia episode as one if at least one early afterdepolarization occurred within the recording period of eight minutes, and as zero otherwise. We then quantified the relationship between the prevalence of arrhythmia and the concentration of dofetilide using a non-linear regression curve with a two-parameter equation. For the perfused hearts, we calculated the percentage of premature ventricular contractions of all heart beats during the last minute of drug administration. We defined ventricular tachycardia as three or more consecutive premature ventricular contractions. We analyzed the data using Student's t-test for normally distributed data with equal variance between groups and the Mann-Whitney U test for all other data. For all analyses, we used Prism 7.

* Data Availability

The data that support the findings of this study are available from the corresponding

author upon reasonable request.

Table 1: **Effect of drugs on ion channels.** IC_{50} values and effective free therapeutic concentration $\mathrm{C_{max}}$ for the 23 drugs used in this study[7].

drug	I_{CaL} IC_{50} [nM]	I_{Kr} IC_{50} [nM]	C_{max} [nM]
ajmaline	71000	1040	900
amiodarone	270	30	0.3
bepridil	211	33	21.5
chlorpromazine	-	1470	20.5
cibenzoline	30000	22600	739
cisapride	-	6.5	3.8
diltiazem	450	17300	87.5
dofetilide	60000	5	1.2
fluvoxamine	4900	3100	196
haloperidol	1700	27	2.4
mexiletine	100000	50000	2787
nifedipine	60	275000	5.4
nitrendipine	0.3	10000	1.6
phenytoin	103000	100000	4250
pimozide	162	20	0.6
prenylamine	1240	65	13
propranolol	18000	2828	19
quinidine	15600	300	2080.5
sertindole	8900	14	0.8
tedisamil	-	2500	80
terfenadine	375	8.9	4.5
thioridazine	1300	33	593.5
verapamil	100	143	53

1. Göktepe, S. & Kuhl, E. Computational modeling of cardiac electrophysiology: A novel finite element approach. *International Journal for Numerical Methods in Engineering* **79**, 156–178 (2009).

2. Wong, J., Göktepe, S. & Kuhl, E. Computational modeling of chemo-electro-mechanical coupling: A novel implicit monolithic finite element approach. *International Journal for Numerical Methods in Biomedical Engineering* **29**, 1104–1133 (2013).

3. O'Hara, T., Virág, L., Varró, A. & Rudy, Y. Simulation of the undiseased human cardiac ventricular action potential: model formulation and experimental validation. *PLoS Computational Biology* **7**, e1002061 (2011).

4. Priest, J. *et al.* Early somatic mosaicism is a rare cause of long-QT syndrome. *Proceedings of the National Academy of Sciences* **113**, 115550–11560 (2016).

5. ten Tusscher, K., Noble, D., Noble, P. & Panfilov, A. A model for human ventricular tissue. *American Journal of Physiol – Heart and Circulation Physiology* **286**, H1573–89 (2004).

6. Zemzemi, N. *et al.* Computational assessment of drug-induced effects on the electrocardiogram: from ion channel to body surface potentials. *British Journal of Pharmacology* **168**, 718–733 (2013).

7. Mirams, G. *et al.* Simulation of multiple ion channel block provides improved early prediction of compounds' clinical torsadogenic risk. *Cardiovascular Research* **91**, 53–61 (2011).

8. Johnstone, R. H., Bardenet, R., Gavaghan, D. J. & Mirams, G. R. Hierarchical bayesian inference for ion channel screening dose-response data. *Wellcome open research* **1** (2016).

9. Sahli Costabal, F., Yao, J. & Kuhl, E. Predicting the cardiac toxicity of drugs using a novel multiscale exposureresponse simulator. *Computer Methods in Biomechanics and Biomedical Engineering* (2018).

10. Sahli Costabal, F., Yao, J., Sher, A. & Kuhl, E. Predicting critical drug concentrations and torsadogenic risk using a multiscale exposure-response simulator (2018).

11. Sahli Costabal, F., Yao, J. & Kuhl, E. Predicting drug-induced arrhythmias by multiscale modeling. *International Journal for Numerical Methods in Biomedical Engineering* **34**, e2964 (2018).

12. Stewart, P. *et al.* Mathematical models of the electrical action potential of Purkinje fibre cells. *Philosophical Transactions: Mathematical, Physical, and Engineering Sciences* **367**, 2225–2255 (2009).

13. Dassault Systèmes, SIMULIA. *Abaqus 2017, Documentation* (Dassault Systèmes, Rhode Island, 2017).

14. Baillargeon, B., Rebelo, N., Fox, D., Taylor, R. & Kuhl, E. The Living Heart Project: A robust and integrative simulator for human heart function. *European Journal of Mechanics. A: Solids* **48**, 38–47 (2014).

15. Costabal, F. S., Matsuno, K., Yao, J., Perdikaris, P. & Kuhl, E. Machine learning in drug development: Characterizing the effect of 30 drugs on the qt interval using gaussian process regression, sensitivity analysis, and uncertainty quantification. *Computer Methods in Applied Mechanics and Engineering* **348**, 313 – 333 (2019).

16. Parikh, J., Gurev, V. & Rice, J. J. Novel two-step classifier for torsades de pointes risk stratification from direct features. *Frontiers in pharmacology* **8**, 816 (2017).

17. Gramacy, R. B. & Polson, N. G. Particle Learning of Gaussian Process Models for Sequential Design and Optimization. *Journal of Computational and Graphical Statistics* **20**, 102–118 (2017).

18. McMillan, B., Gavaghan, D. J. & Mirams, G. R. Early afterdepolarisation tendency as a simulated pro-arrhythmic risk indicator. *Toxicology Research* **6**, 912–921 (2017).

19. Wiśniowska, B. & Polak, S. Am I or am I not proarrhythmic? Comparison of various classifications of drug TdP propensity. *Drug Discovery Today* **22**, 10–16 (2017).